Materials Science and Engineering B 177 (2012) 1423–1429

Contents lists available at SciVerse ScienceDirect

Materials Science and Engineering B

journal homepage: www.elsevier.com/locate/mseb

Structural and photoluminescence study of Er–Yb codoped nanocrystalline ZrO_2–B_2O_3 solid solution

P. Salas [a], R. Borja-Urby [b], L.A. Diaz-Torres [b,*], G. Rodriguez [a], M. Vega [c], C. Angeles-Chavez [d]

[a] Centro de Física Aplicada y Tecnología Avanzada, Universidad Nacional Autónoma de México, A.P. 1-1010, Querétaro 76000, Mexico
[b] Grupo de Espectroscopia de Materiales Avanzados y nanoestructurados (EMANA), Centro de Investigaciones en Óptica, A. C., Loma del Bosque 115, Col. Lomas del Campestre, C.P. 37150 León, Gto., Mexico
[c] Centro de Geociencias, Universidad Nacional Autónoma de México, A.P. 1-1010, Querétaro 76000, Mexico
[d] Instituto Mexicano del Petróleo, Programa de Ingeniería Molecular, Eje Central Lázaro Cárdenas 152, A.P. 14-805, 07730 México, DF, Mexico

ARTICLE INFO

Article history:
Received 30 September 2011
Received in revised form
23 December 2011
Accepted 15 January 2012
Available online 30 January 2012

Keywords:
ZrO_2
B_2O_3
Upconversion
Phase transition
FTIR

ABSTRACT

Codoped Er^{3+} and Yb^{3+} nanocrystalline ZrO_2–B_2O_3 phosphor obtained by a modified sol–gel method is demonstrated. The addition of up to 2.5 mol% B_2O_3 to nanocrystalline ZrO_2:Yb(2%), Er(1%) keep the tetragonal rare-earth stabilized ZrO_2 phase; whereas higher B_2O_3 content destabilize the tetragonal phase, leading to the tetragonal to monoclinic transition with no tetragonal ZrO_2 phase segregation. Visible upconversion of the luminescent active ions, Er^{3+} and Yb^{3+}, depend strongly on B_2O_3 content. The PL intensity is strongly quenched for high B_2O_3 content due to increasing multiphonon relaxation processes related to B—O and B—O—B vibronic modes.

1. Introduction

Upconversion photoluminescent properties of rare earth ions in a variety of hosts have been widely studied for their direct application on the display and the illumination industry [1–4]. Upconversion photoluminescence emissions of rare earth ions are directly affected by the structural vibrations of the host that supports them, diminishing the intensity of the emissions as the vibration or phonon frequency of the host increases. Among a wide variety of hosts, zirconium dioxide (ZrO_2) is one of the best candidates to support rare earth ions because of its low phonon energy of 470 cm^{-1} [5]. Yb^{3+}–Er^{3+} codoped systems are of particular interest since the wide absorption and emission bands of Yb^{3+}, in the range of 870–1060 nm, overlap with that of Er^{3+} ($^4I_{15/2} \rightarrow {}^4I_{11/2}$), allowing efficient energy transfer processes to happen between ytterbium and erbium ions [6,7]. Such interactions in the codoped system enhance the conversion efficiency of near infrared (970 nm) to visible (540 and 660 nm) light, improving the Er^{3+} upconversion emissions. Recently, research studies on ZrO_2:Ce^{3+} conducted by Lee et al. achieved optimization of blue–green photoluminescence emission of this phosphor by addition of B_2O_3 during the synthesis process [8]. They found that boron ions diffusion into the zirconia structure retards the strong segregation of the $Ce_{0.75}Zr_{0.25}O_2$ byproduct for Ce_2O_3 concentrations as high as 5 mol%, whereas without boron doping the same level of $Ce_{0.75}Zr_{0.25}O_2$ segregation is reached at concentrations as low as 2.5 mol% Ce_2O_3. Another research conducted by Rui et al., on borate phosphors, which have low synthetic temperature and low cost, probed $Sr_3RE(BO_3)_4$:Dy^{3+} (RE = Y, La, Gd) to be a potential candidate for white-light generation for UV-pumped white-LEDs [1]. Boron oxide introduction into the yttria-stabilized zirconia probed B_2O_3 to be a fine additive which benefits the sinterability and densification of the samples. Besides, proper concentrations of B_2O_3 allow phase tuning of yttria-stabilized zirconia [9]. In the present research, the influence of boron oxide on the structural and optical properties of the Yb^{3+}–Er^{3+} codoped ZrO_2 system is conducted. Characterization of samples with different content of B_2O_3 is done by XRD, SEM, FTIR and UV–vis absorption. Transition from stabilized tetragonal to monoclinic phase is found at high concentrations of B_2O_3. Upconversion emission of this system is presented as a function of B_2O_3 concentration.

2. Experimental

2.1. Synthesis

Nanocrystals were prepared using the sol–gel method [10]. Six samples of ZrO_2 codoped with 2 mol% Yb^{3+}, 1 mol% Er^{3+}, and xB_2O_3

* Corresponding author. Tel.: +52 477 441 4200; fax: +52 477 441 4209.
E-mail address: ditlacio@cio.mx (L.A. Diaz-Torres).

0921-5107/$ – see front matter © 2012 Elsevier B.V. All rights reserved.
doi:10.1016/j.mseb.2012.01.009

(x = 0, 0.5, 2.5, 5, 10 and 20 mol%) were synthesized. The samples were obtained by mixing zirconium n-propoxide (ZP) in a solution of ethanol (EtOH), nitric and hydrochloric acid at room temperature and vigorous stirring according to the molar rate 1/20/0.1/0.3, respectively. Then the corresponding amounts of boric acid, $Er(NO_3)_3{\cdot}5H_2O$ and $YbCl_3{\cdot}6H_2O$ were added under vigorous stirring and the obtained solution was stirred during 90 min. Then CO_2-free distilled water in a molar rate of 1/4 was added dropwise to manipulate the gel and oxolation processes. Due to the high reactivity of ZP, it was required a strict handling of the hydrolysis process to control the homogeneity, avoid the opacity and precipitation. All samples were aged at 60 °C for 48 h and then at a 100 °C for 24 h. The product was grounded in an agate mortar to obtain a fine powder. Afterwards the samples were heat treated at 500 °C for 5 h, and another set of samples, under the same synthesis process, was heat treated at a 1000 °C for 5 h.

2.2. Characterization

The X-ray diffraction patterns of annealed samples were measured in a θ–θ Bruker D-8 Advance diffractometer having the Braggo-Brentano geometry, Cu Kα radiation, a Ni 0.5% Cu-Kβ filter in the secondary beam and a one-dimensional position sensitive silicon strip detector (Bruker, Lynxeye). Diffraction intensity as a function of the angle 2θ was measured between 20° and 110° with a 2θ of 0.01946° and a counting time of 53 s per point. Crystalline phase composition refinement was done via the Rietveld method and using Fullprof code [11]. Crystalline space groups considered for Rietveld refinement were space group *P42/nmc* for tetragonal ZrO_2, space group *P21/c* for monoclinic ZrO_2, and space group *P63/mmc* for the $LnBO_3$ hexagonal phase. Transmission electron microscopy (TEM) and scanning transmission electron microscopy (STEM), were performed both in a JEM-2200FS microscope with an accelerating voltage of 200 kV. The microscope is equipped with a Schottky-type field emission gun, and an ultra high resolution configuration (Cs = 0.5 mm; Cc = 1.1 mm; point-to-point resolution = 0.19 nm) and in-column omega-type energy filter. High angle annular dark field (HAADF) image was obtained using the HAADF detector in the STEM mode. The optical absorption spectra were obtained with a Perkin-Elmer UV–vis–NIR Lambda 900 spectrophotometer in diffuse reflectance mode using a 1.5 in integrating sphere (Labshpere Co.) Photoluminescence characterization measurements were performed on an Acton Research modular 2300 spectrofluorometer. The excitation source was a CW semiconductor laser diode centered at 970 nm. The emission was analyzed with an Acton Spectra Pro 500i monochromator and a R955 Hamamatsu photomultiplier, connected to an Acton Research Spectra HUB and a PC that collected all data. Photoluminescence measurements were done at room temperature.

3. Results and discussion

X-ray diffraction (XRD) patterns of samples heat treated at 500 °C (Fig. 1) show that at this temperature concentrations of B_2O_3 as high as 20 mol% do not influence the crystalline structure of ZrO_2. All samples have the tetragonal phase, according to JCPDS 50-1089 standard, and there is no detectable segregation of other phases. All reflection peaks are well resolved and intense, which is an indication of the good crystalline structure of these samples. Besides, Rietveld refinement indicates that the small crystallite sizes are in the range from 14.4 up to 16.2 nm. As it is shown by the XRD patterns in Fig. 1, regardless of the B_2O_3 content the overall fixed concentration of rare earths (2% Yb and 1% Er) is the reason for the stable tetragonal ZrO_2 phase, in agreement with previous reports [12–14]. Introduction of B_2O_3 only leads to a slight decrement of peaks intensities as B_2O_3 increases up to 20 mol%. For samples that undergo heat treatment at a 1000 °C it is observed that crystalline structure depends on B_2O_3 content (Fig. 2). Samples with concentrations of 0, 0.5 and 2.5 mol% B_2O_3 preserve pure tetragonal phase and have slight increments of their peaks intensity as B_2O_3 increases. No additional peaks that might indicate segregated phases are observed for these low B_2O_3 concentrations. Hence there is an enhancement of crystal structure on these samples due to removal of organic materials off their structure after heat treatment. On the other hand, higher concentration of boron oxide promote the tetragonal to monoclinic phase transition starting from 5 mol% up to 20 mol% of B_2O_3. XRD patterns of these samples were in agreement to JCPDS 37-1484 standard for monoclinic ZrO_2, and to JCPDS 74-1937 standard for

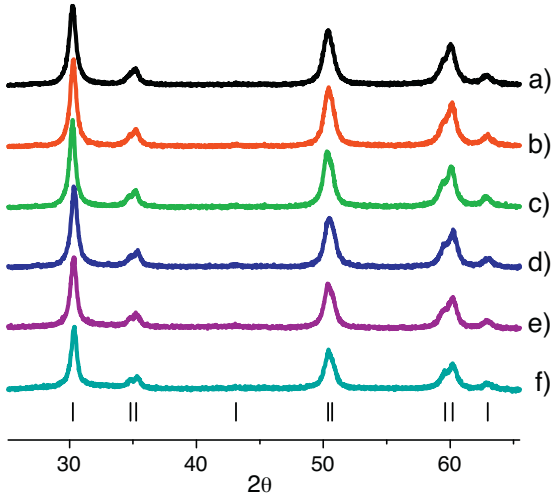

Fig. 1. XRD patterns of samples treated at 500 °C show that despite the increment of boron oxide concentration: (a) 0 mol%, (b) 0.5 mol%, (c) 2.5 mol%, (d) 5 mol%, (e) 10 mol% and (f) 20 mol%, the crystalline structure is tetragonal; in agreement with the JCPDS 50-1089 (bottom lines).

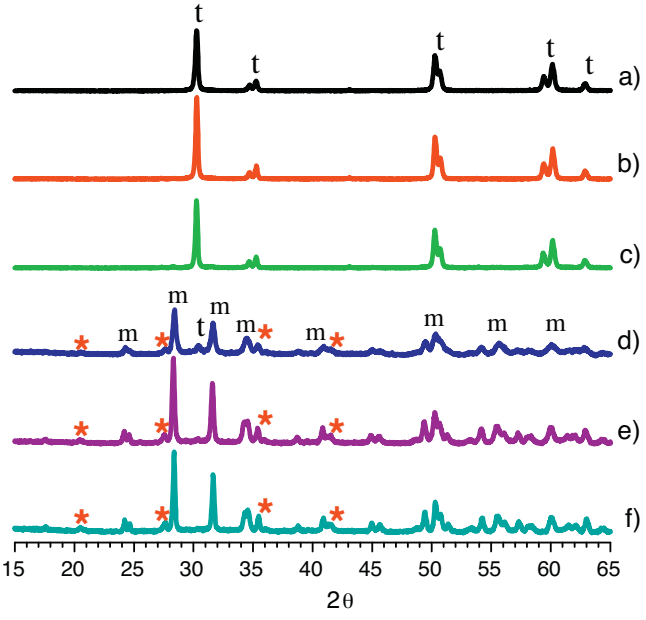

Fig. 2. XRD patterns of samples treated at a 1000 °C and B_2O_3 content: (a) 0 mol%, (b) 0.5 mol%, (c) 2.5 mol%, (d) 5 mol%, (e) 10 mol% and (f) 20 mol%. (t), (m), and (*) stand for the tetragonal and monoclinic ZrO_2 phases, and (*) for the lanthanide borate segregated phase, respectively.

Table 1
Band gap estimations, phase composition: (t) for tetragonal ZrO_2, (m) for monoclinic ZrO_2 and (h) for hexagonal $LnBO_3$, crystallite size and lattice constants from the Rietveld refinement of samples treated at 500 °C and at a 1000 °C.

B_2O_3	Band gap [eV]	Composition [wt%]	Crystallite size [nm]	Lattice constants
500 °C				
0 mol%	4.65	100 (t)	14.41	$a = 3.6092$; $c = 5.1752$
0.5 mol%	4.77	100 (t)	15.6	$a = 3.6086$; $c = 5.1767$
2.5 mol%	4.62	100 (t)	16.1	$a = 3.6085$; $c = 5.1783$
5 mol%	4.59	100 (t)	15.4	$a = 3.609$; $c = 5.1832$
10 mol%	4.78	100 (t)	16.2	$a = 3.6090$; $c = 5.1835$
20 mol%	4.92	100 (t)	15.6	$a = 3.6101$; $c = 5.1840$
1000 °C				
0 mol%	4.83	100 (t)	54.1	$a = 3.6072$; $c = 5.1782$
0.5 mol%	4.83	100 (t)	66.3	$a = 3.6056$; $c = 5.1805$
2.5 mol%	4.86	100 (t)	66.7	$a = 3.6055$; $c = 5.1823$
		13.43 (t)	66.0	$a = 3.6052$; $c = 5.1866$
5 mol%	4.89	81.54 (m)	29.1	$a = 5.1673$; $b = 5.2185$; $c = 5.3221$
		5.04 (h)	39.0	$a = 3.759$; $c = 8.743$
		0 (t)	–	–
10 mol%	4.99	90.87 (m)	53.0	$a = 5.1578$; $b = 5.2119$; $c = 5.3294$
		9.13 (h)	36.0	$a = 3.7585$; $c = 8.746$
		0 (t)	–	–
20 mol%	5.02	88.68 (m)	65.0	$a = 5.1553$; $b = 5.2127$; $c = 5.3276$
		11.32 (h)	36.0	$a = 3.7575$; $c = 8.746$

hexagonal Lanthanide borate. In spite that these samples have the well defined reflection peaks of the ZrO_2 monoclinic phase, there can be seen some other reflection peaks at 20.5°, 27.58°, 34.65° and 41.56°, which do not belong to the monoclinic ZrO_2 phase. Rietveld refinement of these XRD patterns was performed to know the tetragonal and monoclinic phase percentages. In addition, since some peaks were identified as reflections corresponding to the hexagonal phase of segregated lanthanide borates, $LnBO_3$ (Ln = Yb^{3+} or Er^{3+}) [15], such lanthanide borate phase was also included in the Rietveld refinements. Rietveld results are summarized in Table 1. There, it is observed that segregated tetragonal phase exist only at the 5 mol% B_2O_3 sample corresponding to 13.4 wt% of this sample composition, whereas for samples with 10 mol% and 20 mol% B_2O_3, the tetragonal ZrO_2 phase is absent, suggesting that transition to the monoclinic phase is complete. From Table 1 it is clear that lanthanide borate segregation increases from 5.04 to 11.32 wt% as the B_2O_3 content increases from 5 to 20 mol% of B_2O_3 respectively. Affinity between boron and rare earth ions and yttrium ions has been previously reported [9,15]. de Florio et al. conducted experiments on Yttria-stabilized zirconia and used boron oxide as an additive. Their results showed that phase composition tuning (cubic + monoclinic) is possible by proper addition of B_2O_3. Boron ions destabilize the cubic phase by removal of yttrium ions from the $YZrO_2$ lattice to form the YBO_3 segregated phase. Such destabilization in turns induced a strong transition to monoclinic phase [9]. Thus, Rietveld refinements of XRD patterns in Fig. 2 suggest that boron ions diffuse well into the rare earth stabilized tetragonal phase of the host (ZrO_2:Yb^{3+}, Er^{3+}) but do not lead to enough amounts of $LnBO_3$ compounds as to induce destabilization of the tetragonal ZrO_2 phase. Whereas for B_2O_3 concentrations of 5 mol% B_2O_3 and higher, up to 20 mol%, boron ions interact strongly with rare earth ions. Extracting these from the tetragonal structure to form lanthanide borate crystallites of considerable size, around 36 nm, see Table 1. After rare earth ions extraction, the tetragonal ZrO_2 crystalline structure is destabilized allowing in turn the transition to the monoclinic ZrO_2 phase.

The morphological and structural characteristics of the sample with 5 mol% of B_2O_3 were analyzed by TEM and the results obtained are displayed in Fig. 3. The sample is composed by particles of different sizes and very well faceted as displayed in HAADF image of Fig. 3a. The HAADF detector collects electrons dispersed by the nucleus of atoms and its intensity is approximately the squared of atomic number. Therefore, electrons dispersed by the heavier elements are more intense than the electrons dispersed by the lighter elements producing brighter dots in a HAADF image. As can be observed in the HAADF image, the particles show similar contrast suggesting only presence of ZrO_2 particles. Less bright or dark particles that could correspond to lighter compounds B_2O_3 or $LnBO_3$ were not observed in the HAADF image. Subsequently, the crystal structure of less bright particles in the HAADF image (Fig. 3a) was studied by obtaining images of atomic resolution. Fig. 3b displays a HRTEM image corresponding to a thin section of one of such particles and the crystal lattice of the particle is clearly revealed. In the HRTEM image, the crystal planes show a discontinuity in the direction indicated by the white arrow. The discontinuity indicates an increase in the thickness in the direction of the arrow. Therefore, crystal structure was analyzed in a thinner region, indicated by the inset A in Fig. 3b. The determination of the crystal structure was performed on the Fast Fourier Transform (FFT), Fig. 3c; it was obtained for the inset A of Fig. 3b. Interplanar distances of 0.295, 0.289 and 0.255 nm were obtained in the FFT. These values match very well with the interplanar spacing of tetragonal zirconia phase reported in the (Join committee Powder Diffraction Standard) JCPDS card no 50-1089. The *d*-spacing correspond to (0 1 1), (0 −1 1), and (0 0 2) planes of the tetragonal zirconia phase viewed along the crystallographic axis [1 0 0]. The corresponding inverse FFT image is illustrated in Fig. 3d, displaying clearly the crystal lattice in the [1 0 0] direction.

The presence of absorption bands corresponding to transitions from the ground state to corresponding excited states of Yb^{3+} and Er^{3+} ions are patent in the absorption spectra of samples annealed at 1000 °C. The corresponding final exited states are indicated in Fig. 4a for the sample with 5 mol% B_2O_3 content. Evidence of occluded H_2O within the crystallites is observed at the 1386 nm absorption band for all samples after the annealing treatment at a 1000 °C (Fig. 4a). It is observed a red shift of the UV edge of the absorption spectra of Er–Yb codoped ZrO_2 as B_2O_3 content increases. In particular for the 20 mol% B_2O_3 sample a very clear broad band centered on 400 nm can be observed. That band and increased absorption for short wavelengths could be a consequence of increasing defects within the crystallites induced by the segregation of the lanthanide borate phase, in correspondence with the XRD patterns of highly doped samples. Introduction of B_2O_3 enhance the absorption properties of the rare earth ions in these samples. As B_2O_3 content increases, it is observed an increment in intensity and a better definition of the absorption bands of Er^{3+} in

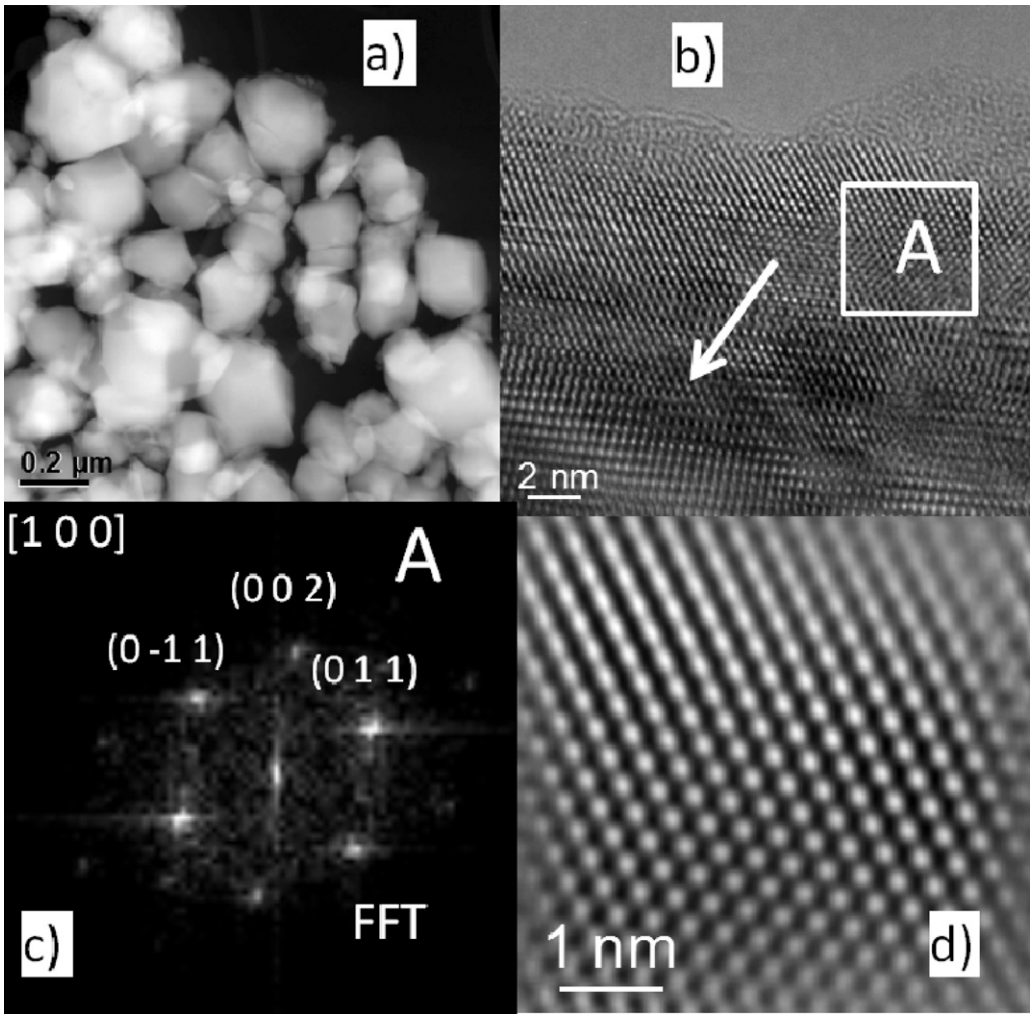

Fig. 3. Morphology and structure of the sample with 5 mol% B_2O_3: (a) HAADF image of different size polyhedral nanoparticles very well dispersed, (b) HRTEM image, (c) crystal structure of the box A in HRTEM image (b), and its Fourier transform pattern (d).

the visible as well as the band related to the $^4I_{11/2}$ (Er^{3+}) and $^2F_{5/2}$ (Yb^{3+}) excited states near 970 nm. The information of the absorption spectra was transformed to Munk–Kubelka units to estimate the optical bang gap energy (Eg). The estimations were based on the relation: $(\alpha h\nu)^2 = C(h\nu - \mathrm{Eg})$; where α is the absorption coefficient, $h\nu$ is the photon energy in eV and C is a constant. These spectra are displayed in a Wood and Tauc plot [12] in Fig. 5. Extrapolation of a straight line from the band edge to the intersection with $h\nu$ axis gives the band gap estimation. It was found the Eg grows as boron oxide concentration increases in the samples annealed to 1000 °C, see Table 1. Despite being crystalline, samples of tetragonal phase ($x \leq 2.5$ mol%) have lower band gap energy (Eg = 4.83 eV) because of more incomplete metal—oxygen (M—O) bonds in their less ordered structure [16], in comparison with the more ordered structures of the monoclinic phase samples ($x \geq 5$ mol%) with higher band gap energy (Eg = 5.02 eV).

Taking in to account that the phononic energy of pure ZrO_2 is around 470 cm^{-1}, which place it as one of the best host to insert rare earth ions for upconversion photoluminescence (PL) applications [5], FTIR was performed to look for boron bonds inside the crystalline structure, and see how boron introduction affects the phononic energy distribution of these materials. For the sample without B_2O_3, annealed at 1000 °C, the principal transmittance band is centered at 490 cm^{-1}, which includes the reported 470 cm^{-1} value for bulk ZrO_2, see curve (i) in Fig. 6a. Upon boron introduction this principal band at 490 cm^{-1} shifts to longer wavenumbers at 500 cm^{-1}, this change allows higher phononic energy to happen in the samples ($x \leq 2.5$ mol%), and it is the first indication of boron ions inside the structure, see Fig. 6a. As boron ions increases, the main band sharps itself and shifts to longer wavenumbers. Also, new well defined bands at 418, 580 and 740 cm^{-1} become distinguishable as B_2O_3 increases. Such new bands are related to B_2O bonds and bending vibration of BO_3 [17]. Particularly, the new band at 418 cm^{-1} though it is narrow, it gains considerable intensity. For samples with higher concentrations of B_2O_3 ($x \geq 5$ mol%) and annealing treatment at 1000 °C, the main band continue shifting towards bigger wavenumbers up to 530 cm^{-1} for the 20 mol% B_2O_3 content, see Fig. 6b. The bending vibrations of B—O—B triangles (740 cm^{-1}) gain importance in these systems, becoming a highly probable path for deexcitation processes to happen. Effects of boron ions in the highly doped samples become clear as many resonant vibration bands appear in the FTIR spectra, mainly in the range from 880 to 1200 cm^{-1}, related to stretching vibration of BO_4. Similar bands were also present on a study conducted by Cheng et al., over the influence of rare earth ions on Bi_2O_3–B_2O_3 glasses [17]. Such an increment of vibration bands increases the probability for the system to lose its excited energy via multiphononic vibrations.

The typical green ($^4S_{3/2} \rightarrow {}^4I_{15/2}$) and red ($^4F_{9/2} \rightarrow {}^4I_{15/2}$) upconversion emissions of the Yb^{3+}–Er^{3+} codoped ZrO_2 system are

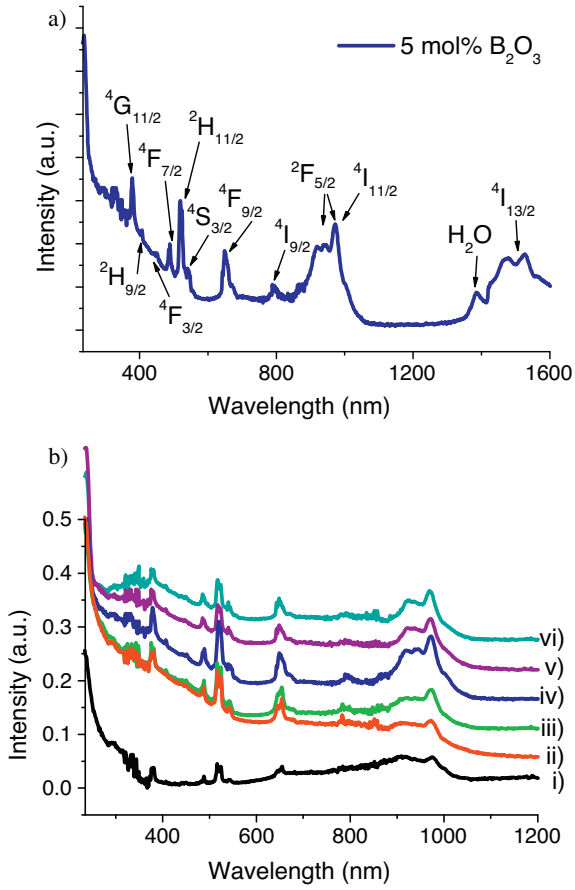

Fig. 4. (a) Absorption band transitions of Er^{3+} and Yb^{3+} from ground states to respective excited energy levels for ZrO_2:Er, Yb sample with 5 mol% content of B_2O_3. (b) Absorption spectra of ZrO_2:Yb^{3+} Er^{3+} xB_2O_3 samples treated at 1000 °C: (i) x = 0 mol%, (ii) x = 0.5 mol%, (iii) x = 2.5 mol%, (iv) x = 5 mol%, (v) x = 10 mol% and (vi) x = 20 mol%.

observed in all samples under 970 nm diode laser excitation. Fig. 7 depicts the upconversion emission spectra for samples annealed at 500 °C, and Fig. 8 depicts the upconversion spectra for samples annealed at 1000 °C. The red emission is predominant in all samples treated at 500 °C, see Fig. 7. The overall upconversion emission intensity presents around a six fold increment with the addition B_2O_3 in comparison with sample without B_2O_3, with exception of the 20 mol% B_2O_3 sample for which its

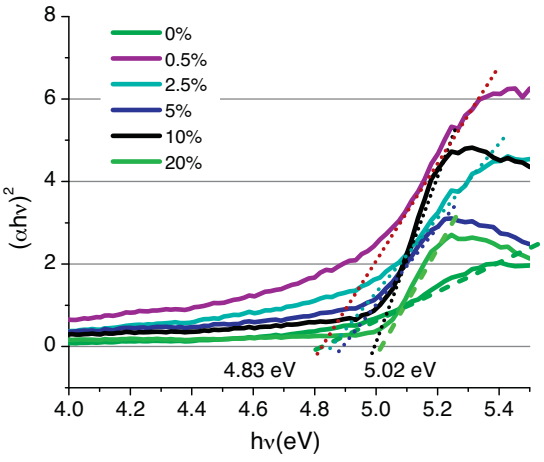

Fig. 5. Tauc plot for the diffuse reflectance in Kubelka–Munk (k/s) units and estimation of band gaps. Percentages on labels correspond to the mol% content of B_2O_3.

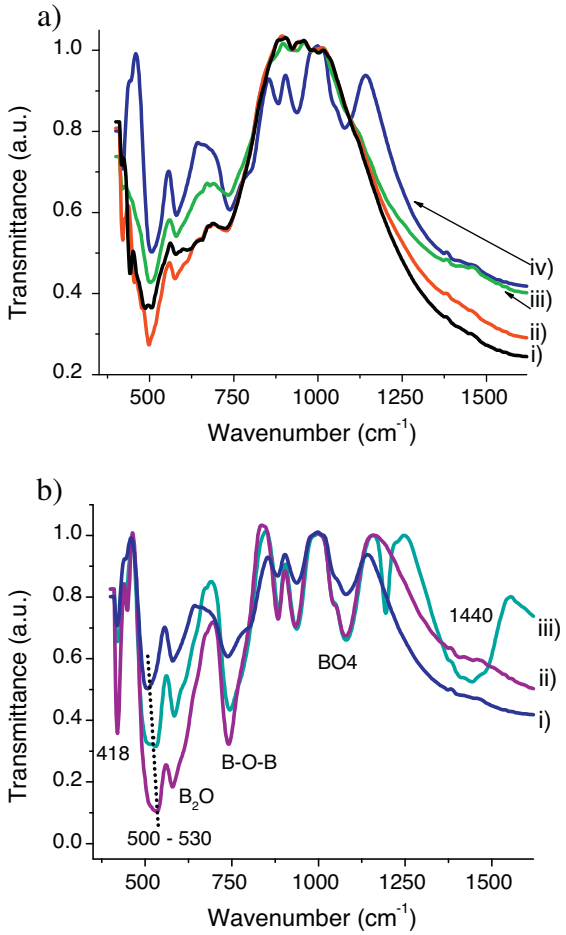

Fig. 6. FTIR spectra of Yb^{3+}, Er^{3+} codoped $ZrO_2 + xB_2O_3$ treated at 1000 °C: (a) samples with boron oxide concentration of: (i) x = 0 mol%, (ii) x = 0.5 mol%, (iii) x = 2.5 mol% and (iv) x = 5 mol%; and (b) samples with (i) x = 5 mol%, (ii) x = 10 mol% and (iii) x = 20 mol%.

upconversion emission is strongly quenched. While being all of them of tetragonal phase, it is observed that the increment on upconverted emissions is not linear with B_2O_3 content. The main vibronic band of the 20 mol% B_2O_3 sample at 1330 cm^{-1} becomes wider and more intense than the band at 500 cm^{-1} allowing multiphononic vibrations of B—O bonds at 1330 cm^{-1} that lead to very strong multiphonon relaxation processes in all Er^{3+} excited levels, see the nonradiative relaxation processes W_i (i = 1, 2, 3, 4) depicted in Fig. 9. As a consequence the overall upconversion emission of such sample is strongly quenched.

In the case of samples treated at a 1000 °C, the overall upconversion emission increases as B_2O_3 content increases up to 5 mol% (Fig. 8), and then is strongly quenched for higher B_2O_3 contents. Sample with 5 mol% B_2O_3 presents the highest increment in overall upconversion emission with around 70% more integrated emission than the sample with no B_2O_3. The gained intensity of the resonant vibration bands at 740 cm^{-1} and 1440 cm^{-1} in the FTIR spectrum, see Fig. 6b, is the reason for strong multiphonon relaxation and consequent upconversion emission quenching for the 10 and 20 mol% B_2O_3 samples. An interesting feature of all samples annealed at 1000 °C is the evident change in the red to green emission ratio in comparison with samples annealed at 500 °C. The green band emission becomes stronger than the red band emission as B_2O_3 content increases up to 5 mol% B_2O_3. And for the higher B_2O_3 contents, in spite that the overall upconversion emission is strongly quenched, the green emission is the dominant one. It is also worth to point out that, a threefold increment in overall upconversion emission is

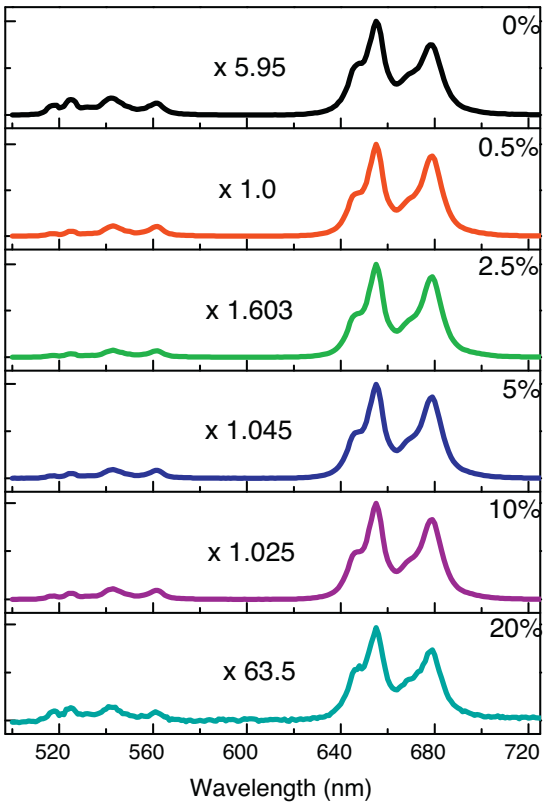

Fig. 7. Green and red upconversion emissions of ZrO_2:Yb^{3+} Er^{3+} xB_2O_3 treated at 500 °C, as a function of boron oxide concentrations x = 0, 0.5, 2.5, 5, 10 and 20 mol%. PL intensities were multiplied by a normalization factor for display purposes to show intensity variations between the samples. The normalization factor is in reference to the integrated PL of sample with 0.5 mol% content of B_2O_3.

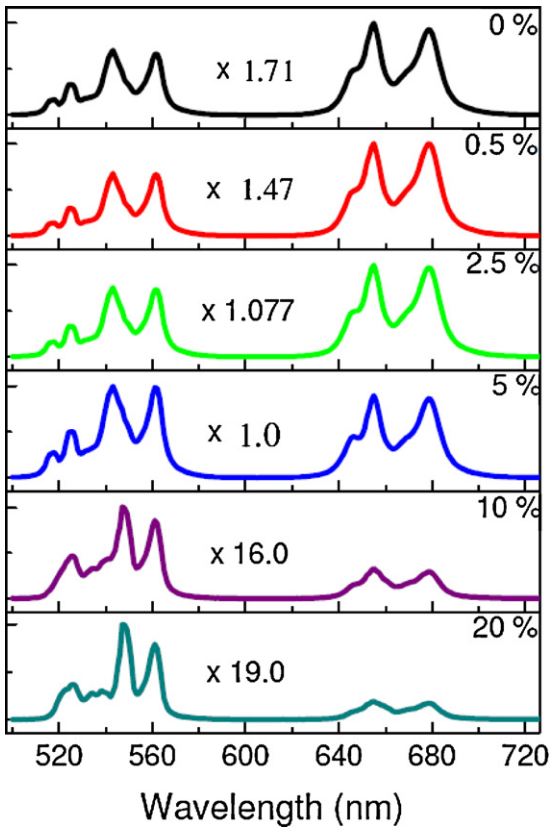

Fig. 8. Green and red upconversion emissions of ZrO_2:Yb^{3+} Er^{3+} xB_2O_3 treated at a 1000 °C, as a function of boron oxide concentrations x = 0, 0.5, 2.5, 5, 10 and 20 mol%. PL Intensities were multiplied by a normalization factor for display purposes to show intensity variations between the samples. The normalization factor is in reference to the Integrated PL of sample with 5 mol% content of B_2O_3.

observed in the samples annealed at 1000 °C in comparison with the ones annealed at 500 °C.

The above results suggest that for the compounds of tetragonal phase (B_2O_3 content ≤ 2.5 mol%) introduction of B_2O_3 leads to diffusion of rare earth ions into the surface of the tetragonal compounds; exposing the RE ions to stronger first neighbors interactions and hence increasing their upconversion emissions, as can be seen in Fig. 8. On the other hand, high concentrations of B_2O_3 promote the tetragonal to monoclinic transition by increasing the lanthanide borate segregation. The rare earth extraction from the monoclinic ZrO_2 phase leads to a very small green upconversion emission as expected in low Er^{3+} doped monoclinic ZrO_2 [6], whereas the extracted rare earth that have been incorporated in the lanthanide borate phase are unable to present upconversion emission due to high boron phononic vibrations energies, as shown in the FTIR spectra in Fig. 6. Those resonant vibration bands of high energy promote de-excitation processes of Er^{3+} excited electrons lo lower excited states disfavoring upconversion emissions.

A schematic energy level diagram of the Yb^{3+}–Er^{3+} codoped ZrO_2 system is shown in Fig. 9, to describe the VIS upconversion and NIR downconversion emission processes. First, the continuous pumping excitation from the laser diode at 970 nm is mainly absorbed by Yb^{3+} ions due to its wide absorption cross section ($^2F_{7/2}$, $^2F_{5/2}$) [6]. Erbium ions are excited from the ground state $^4I_{15/2}$ to the $^4I_{11/2}$ level through direct non-radiative energy transfer (ET) process from ytterbium Yb($^2F_{5/2}$, $^2F_{7/2}$) → Er($^4I_{15/2}$, $^4I_{11/2}$), as well as by direct laser diode excitation to a much lesser degree. Electrons in the $^4I_{11/2}$ level are then excited to the $^4F_{7/2}$ level by a second ET process, Yb($^2F_{5/2}$, $^2F_{7/2}$) → Er($^4I_{11/2}$, $^4F_{7/2}$). Electrons in $^4F_{7/2}$ level rapidly relax to the lower levels $^4S_{3/2}$ and $^2H_{11/2}$

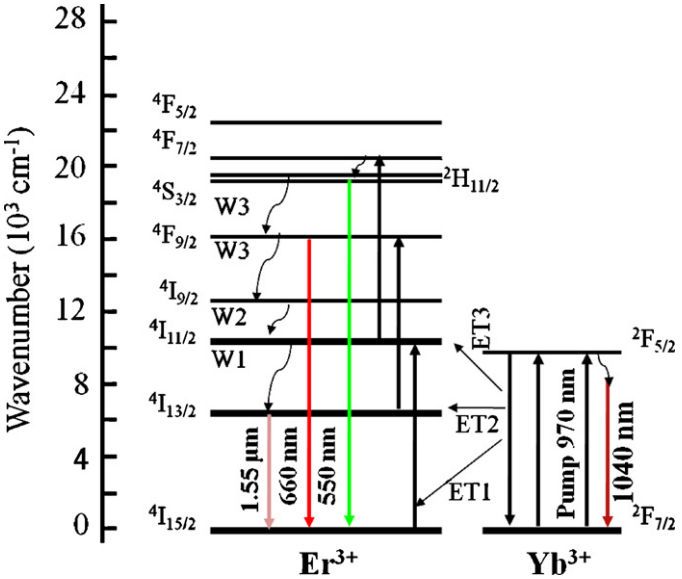

Fig. 9. Schematic energy level diagram for green and red upconversion and infrared emissions of Yb^{3+}, Er^{3+} codoped ZrO_2 + xB_2O_3 under 970 nm diode laser excitation. Erbium is excited via energy transfer (ET) processes. Resonant vibration modes of boron bonds favor nonradiative relaxation of erbium ions (W_i, curved arrows) to lower energy levels.

from which the green upconversion emission (550 nm) is produced when these radiatively relax to the ground state. Also, excited electrons at $^4I_{11/2}$ level decay nonradiatively to the $^4I_{13/2}$ level, from which NIR emission (1550 nm) of Er^{3+} ions takes place. Finally, electrons at $^4I_{13/2}$ level could be excited to $^4F_{9/2}$ level by a third ET process Yb($^2F_{5/2}$, $^2F_{7/2}$) → Er($^4I_{13/2}$, $^4F_{9/2}$), and the red upconversion emission (660 nm) takes place after radiative transitions from this level to the ground state $^4I_{15/2}$ [7,18]. The wide principal vibration band centered at 610 cm^{-1}, see FTIR spectra in Fig. 6, enhances the multiphonon nonradiative relaxation of level $^2H_{11/2}$–$^4S_{3/2}$ to the next lying level $^4F_{9/2}$. That is due to the fact that an increase in the maximum phonon energy from 470 to 610 cm^{-1} will lead to need less phonons to bridge the energy gap between consecutive energy levels, and in consequence the rate for multiphonon relaxations will increase. Likewise the excited electrons at $^4F_{9/2}$ level will decay more nonradiatively to the $^4I_{9/2}$ level, and so on for the rest of the lower lying excited levels. Taking in to account that, the addition of B_2O_3 gives place to the important boron related FTIR bands at 410, 610, 740, and 1440 cm^{-1}, it will be expected an increase in the nonradiative relaxations W_1, W_2, and W_3 (Fig. 9) between energy levels $^4I_{9/2}$ and $^4I_{11/2}$, $^4F_{9/2}$ and $^4I_{9/1}$ and $^4I_{11/2}$ and $^4I_{13/2}$, respectively. As a consequence, the decay rate of an excited electron to the immediate inferior energy level increases, and the emission intensity decreases. Since the $^4I_{11/2}$ level is being populated by relaxed electron from the more energetic levels due to multiphonon relaxations and by direct ET from ytterbium ions, then a more intense red upconversion emission is sustain until the vibration band at 740 cm^{-1} starts to compete with the main vibration band at 500–530 cm^{-1}. That is the case for samples with high concentration of boron oxide. In particular, the 5 mol% B_2O_3 sample shows in its FTIR spectrum an increment of the band at 740 cm^{-1}. Also the PL emission spectrum of this sample shows that the reason between the green and the red band is close to one. Evidencing the system has reached a balance between nonradiative decays and ET processes. Such a balance is lost after increasing the B_2O_3 concentration in the samples (10 and 20 mol%): thus the appearance of more energetic vibration bands (880–1440 cm^{-1}) and their phononic vibration filling the gap between $^4I_{13/2}$ and $^4I_{15/2}$ levels leads to increased nonradiative relaxation of electrons to the ground state $^4I_{15/2}$, that in turn quench almost all radiative emissions.

4. Conclusions

Nanophosphors of Yb^{3+}–Er^{3+} codoped ZrO_2 were synthesized via a sol–gel method, different concentrations of B_2O_3 were introduced during the synthesis process, and two set of samples were heat treated at 500 °C and at a 1000 °C for 5 h each. Structural and optical properties of these nanophosphors were studied as a function of B_2O_3 concentration. Samples treated at 500 °C shown no effect of Boron content on the stabilization of the tetragonal phase, and present a dominant red upconversion emission. Enhancement of upconversion emission is observed after boron oxide introduction and heat treatment at a 1000 °C, in particular the green emission becomes comparable to the red emission. The enhanced tetragonal crystalline structure is preserved for concentrations as high as 2.5 mol% of B_2O_3 without other phase segregations. For higher concentrations of boron oxide, a transition from tetragonal to monoclinic ZrO_2 phase was observed along with lanthanide borate segregation. This phase transition is ascribed to extraction of rare earth ions from the ZrO_2 structure by boron ions. More intense green emissions of samples with low concentrations of boron oxide could be due to the presence of rare earth ions on the surface of the nanophosphors. A schematic energy level diagram is proposed to explain how high concentrations of B_2O_3 kill the upconversion emission of the samples after the increment of resonant vibration bands of boron–oxygen bonds observed in the FTIR spectra.

Acknowledgments

One of the authors, Borja-Urby, thanks to CONACyT for its support through a scholarship grant 173046 for PhD studies at Centro de Investigaciones en Optica A. C.

References

[1] Z. Rui, W. Xiang, J. Alloys Compd. 509 (2011) 1197–1200.
[2] R. Borja-Urby, L.A. Diaz-Torres, P. Salas, C. Angeles-Chavez, O. Meza, Mater. Sci. Eng. B 176 (2011) 1388–1392.
[3] L. Guo, X. Wang, C. Zhong, L. Li, J. Am. Ceram. Soc. 94 (2011) 3175–3177.
[4] M.L. Singla, M. Muhamed Shafeeq, Manish Kumar, J. Lumin. 129 (2009) 434–438.
[5] E. De la Rosa, D. Solis, L.A. Diaz-Torres, P. Salas, C. Angeles-Chavez, O. Meza, J. Appl. Phys. 104 (2008) 103508.
[6] X. Zhang, T. Xu, Q. Nie, S. Dai, X. Shen, X. Zhang, J. Rare Earths 24 (2006) 771–776.
[7] L.A. Diaz-Torres, O. Meza, D. Solis, P. Salas, E. De la Rosa, Opt. Lasers Eng. 49 (2011) 703–708.
[8] C.-M. Lee, Y.-H. Pai, T.-P. Tang, C.-C. Kao, G.-R. Lin, F.-S. Shieu, Mater. Chem. Phys. 119 (2010) 15–18.
[9] D.Z. de Florio, R. Muccillo, Mater. Res. Bull. 39 (2004) 1539–1548.
[10] P. Salas, C. Angeles-Chavez, J.A. Montoya, E. De la Rosa, L.A. Diaz-Torres, H. Desirena, A. Martinez, M.A. Romero-Romo, J. Morales, Opt. Mater. 27 (2005) 1295–1300.
[11] Rodriguez-Carvajal, J. Phys. B 192 (1993) 55–69.
[12] P. Salas, C. Angeles-Chavez, J.A. Montoya, E. De la Rosa, L.A. Diaz-Torres, H. Desirena, A. Martinez, M.A. Romero-Romo, J. Morales, Opt. Mater. 27 (2005) 1295–1300.
[13] D. Solis, T. López-Luke, E. De la Rosa, P. Salas, C. Angeles-Chavez, J. Lumin. 129 (2009) 449–455.
[14] W. Cordova-Martinez, E. De la Rosa-Cruz, L.A. Diaz-Torres, P. Salas, A. Montoya, M. Avendaño, R.A. Rodriguez, O. Barbosa-Garcia, Opt. Mater. 20 (2002) 263–271.
[15] J. Ma, Q. Wu, Y. Chen, Y. Chen, Solid State Sci. 12 (2010) 503–508.
[16] L.S. Cavalcante, J.C. Sczancoski, V.M. Longo, F.S. De Vicente, J.R. Sambrano, A.T. de Figueiredo, C.J. Dalmaschio, M. Siu Li, J.A. Varela, E. Longo, Opt. Commun. 281 (2008) 3715–3720.
[17] Y. Cheng, H. Xiao, W. Guo, Mater. Sci. Eng. A 480 (2008) 56–61.
[18] O. Meza, L.A. Diaz-Torres, P. Salas, E. De la Rosa, D. Solis, Mater. Sci. Eng. B 174 (2010) 177–181.